# Shock Wave Structure in Lennard-Jones Crystal via Molecular Dynamics

V. V. Zhakhovskiĭ and S. V. Zybin
*Institute for High Temperatures, Russian Academy of Sciences, Izhorskaya 13/19, 127412 Moscow, Russia*

K. Nishihara
*Institute of Laser Engineering, Osaka University, 2-6 Yamada-oka, Suita, Osaka 565-0871, Japan*

S. I. Anisimov
*Landau Institute for Theoretical Physics, Russian Academy of Sciences, 117334 Moscow, Russia*
(Received 11 January 1999)

The molecular dynamics (MD) method is applied to study the internal structure of strong steady shock waves in a Lennard-Jones crystal. We develop two different approaches to MD shock simulation which enable us to calculate fine-grained profiles of flow variables and their fluctuations in close detail. In contrast to shock waves in gases and fluids, solid shocks exhibit oscillatory profiles within the shock front. We study in detail these oscillations by exploring the evolution of velocity distribution, pair distribution, and potential energy distribution functions across the shock layer.

PACS numbers: 62.50.+p, 02.70.Ns, 47.40.Nm, 82.40.Fp

Understanding the internal structure of a shock wave is crucial to the development of appropriate continuum constitutive models as well as theoretical treatments of shock-induced phenomena, such as detonation. Previous theoretical studies based either on the linear hydrodynamic approximation [1,2] (which is valid for weak shock waves only) or on the Boltzmann kinetic equation [3,4] (which holds for rarefied gases only) have considered just certain limiting cases. Recently, the direct Monte Carlo and molecular dynamics (MD) simulations have been employed to gain insight into the shock wave structure in dense gases and liquids [5–9] and to test different theoretical approaches [9–12] (see also the review by Holian [13] and references therein). With shock waves in solids, MD simulations demonstrated that the microscopic mechanism of their propagation is inherently more complex because plastic flow is governed by the creation and motion of defects, not by viscous dissipation as in fluids [14–18]. In early simulations of the plastic deformation under shock loading, the creation of dislocations within the shock front has been found [17,18]. Besides, the oscillations of shock wave profiles in the crystalline solid have been reported [15,16], although not observed in subsequent studies (presumably due to the coarse grained averaging grid used to reduce the noise). Nevertheless, some intrinsic features of the shock front structure, including evolution of the kinetic and potential energy distribution functions, have not been previously investigated. To obtain fine-grained averages, Klimenko and Dremin [15] developed a "moving analytical window" technique, which allowed them to calculate the velocity distribution function, but the number of atoms in their simulation was insufficient for quantitative description. In this paper, we implement two specially developed different techniques for MD shock simulation to obtain fine-grained averages and present computer experimental results that shed light on the shock wave structure in solid Lennard-Jonesium.

In our MD simulation the atoms interact via Lennard-Jones (LJ) pair potential with cutoff at $r_c = 2.5\sigma$:

$$\phi_{\mathrm{LJ}}(r) = 4\epsilon[(\sigma/r)^{12} - (\sigma/r)^6] \qquad \text{if } 0 < r \le r_c\,. \tag{1}$$

Hereafter, we use as MD units a fraction of the atomic mass $m/48$ and the LJ parameters $\sigma$ and $\epsilon$. The units of time $\tau$ and velocity $\nu$ are then $\sigma\sqrt{m/48\epsilon}$ and $\sqrt{48\epsilon/m}$, respectively. For argon atoms $\sigma = 3.405 \times 10^{-10}$ m, $\epsilon/k_B = 119.8$ K, $\tau = 3.113 \times 10^{-13}$ s, $\nu = 1094$ m/sec, and the units of density and pressure are 1680.4 kg $/\mathrm{m}^3$ and 41.9 MPa. Besides, we devised a modification of LJ potential by addition a cubic polynomial in $r^2$ to make both the potential energy and the force decay smoothly to zero at $r_c$. The modified $\mathrm{LJ}_{\mathrm{smooth}}$ potential with the same minimum $\epsilon$ at $r_0 = 2^{1/6}\sigma$ is given by

$$\begin{aligned} \phi(r) &= \phi_{\mathrm{LJ}}(r) - a_2(r^2 - r_0^2)^2 - a_3(r^2 - r_0^2)^3, \\ a_2 &= -3.528901 \times 10^{-3}, \\ a_3 &= 5.758681 \times 10^{-4}, \end{aligned} \tag{2}$$

with $a_2$ and $a_3$ (in units of $\sigma$ and $\epsilon$) chosen such that $\phi(r_c) = 0$, $\phi'(r_c) = 0$. For $r = r_0$, $\phi'(r_0)$ is also zero. The resulting expressions for $a_2$ and $a_3$ are

$$\begin{aligned} a_2 &= \frac{3\phi_c}{(r_c^2 - r_0^2)^2} - \frac{\phi_c'}{2r_c(r_c^2 - r_0^2)}, \\ a_3 &= \frac{\phi_c}{(r_c^2 - r_0^2)^3} - a_2\,, \end{aligned} \tag{3}$$

with $\phi_c = \phi_{\mathrm{LJ}}(r_c), \phi_c' = \phi_{\mathrm{LJ}}'(r_c)$. The $\mathrm{LJ}_{\mathrm{smooth}}$ potential approaches conventional LJ potential as $r_c$ tends to infinity. The main advantages of the proposed modification are a better energy conservation and elimination of

  

discontinuities at $r = r_c$, which is particularly important when applying a high order integration method.

Two different ways have been employed to simulate a planar shock wave in a three-dimensional crystal composed of atoms initially placed in perfect face-centered-cubic (fcc) lattice sites. A shock wave is made to propagate in the $\langle 001 \rangle$ direction along the $z$ axis. The first technique previously developed in Ref. [8] is intended for steady shock waves, where the computational MD cell $L_x \times L_y \times L_z$ with periodic boundary conditions in the $x$ and $y$ directions is essentially centered on the shock front at rest. Uncompressed lattice planes are fed into the MD cell from the right ($z > 0$) at upstream shock velocity $u_0 = -u_s$, while a finite-magnitude piston potential $\phi_p$ on the left side ($z < 0$) slows down the particles to downstream velocity $u_1 = -u_s + u_p$ causing shock compression. The potential $\phi_p$ must satisfy the condition $\partial\phi_p/\partial z = 0$ at the left boundary $z = -L_z/2$ of the cell. It is possible to control the compression and the strength of a shock wave by adjusting the magnitude of piston potential. To form a uniform upstream flow with initial temperature $T_0$ and mass velocity $u_0$, the Langevin thermostat is applied on the right side of the MD cell in which the particles are subjected to the Langevin force: $dv_{ik}/dt = -\beta(u_0\delta_{kz} + v_{ik}) + \xi_k(t)$, $k = x, y, z$, where $\beta$ is the friction coefficient and $\xi_k(t)$ is the Gaussian random force. To obtain a prescribed temperature $T_0$, these parameters should satisfy the condition $\langle \xi_k^2 \rangle = 2\beta T_0/h$, where $h$ is a time step. Furthermore, an additional thermostat is used to absorb the outgoing particles on the left side. This technique has been applied to obtain time averages. The second way is intended for measuring ensemble averages and can be used for simulation both of steady and of nonsteady shock waves. It consists in taking an average over repeated simulations with randomly generated initial positions and velocities of particles constituting independent systems from an ensemble. Shock wave in the fcc lattice at rest is initiated by causing the piston particles at the left boundary of the MD cell to move at a steady velocity $u_p$ toward the right ($z > 0$). During the movement the piston particles are constrained to remain at their moving lattice sites (infinitely massive cold piston) or else to maintain their mean velocity in the $z$ direction constant: $\langle v_z \rangle = u_p$ (heated piston). As the shock wave moves away from the piston, the leftmost piston planes are removed while new lattice planes are appended at the right boundary. This allows the length of the computational cell to be kept at around $L_z$.

The dimensions of the MD cell were 32 by 32 fcc unit cells in square cross-sectional area (2048 atoms in transverse planes) and about 100 lattice planes in length along the shock propagation direction. The parameters of simulated shock waves are listed in Table I. The spatial profiles of averaged quantities are generated by partitioning the $z$ axis into small bins of the width $\sim 0.1\sigma$. In our simulations, we employed both time-averaging and ensemble-averaging techniques. In addition, the moving analytical window technique from Ref. [15] has been used for comparison. The profiles obtained by the three different techniques are in close agreement.

TABLE I. Parameters of shock waves in MD experiments. The initial density $\rho_0 = 1.048$, $c_0 = (72\epsilon/m)^{1/2}$ is 1D longitudinal sound speed, $\tau_{\max}$ is the maximum shear stress, and $\Delta P$ is the Hugoniot jump in pressure behind the shock front.

| Run | $u_p/c_0$ | $u_s/c_0$ | $\rho_1/\rho_0$ | $T_0$ | $T_1$ | $\Delta P/\tau_{\max}$ |
|---|---|---|---|---|---|---|
| *A* | 1.45 | 4.0 | 1.57 | 0.18 | 18.7 | 13.0 ± 1 |
| *B* | 1.19 | 3.4 | 1.53 | 0.18 | 12.4 | 16.0 ± 1 |

Figure 1 shows these profiles for run *A*. The distinctive feature of shock waves in LJ crystal is an oscillatory structure of profiles within the shock front. Similar phenomenon has been also observed in early time-averaging MD simulations [15,16]. It can be attributed to the fact that the plastic deformation and transformation of the energy of ordered motion along the $z$ axis into energy of random (thermal) motion along the $x$ and $y$ axes proceed slowly, and the wave behaves at the beginning of the shock front as though the lattice was nearly one dimensional. However, unlike the nonsteady soliton train in 1D lattices [14], the oscillatory structure in 3D shock waves is steady even for weak shocks at low initial temperature [19]. Behind the oscillation region, the melting transition has occurred (in run *A*) accompanied by the shock front spreading [20] with relaxation of the shear stress to zero.

Since the kinetic energy distribution within the shock front is nonequilibrium, we use the mean-square fluctuations of the longitudinal $v_z$ and transverse $v_x, v_y$ components of the particle velocity given by $T_{xx} = 48\langle v_x^2 \rangle$, $T_{yy} = 48\langle v_y^2 \rangle$, and $T_{zz} = 48\langle (v_z - u_z)^2 \rangle$ as kinetic temperature components which are equal to the thermodynamic temperature $T$ at equilibrium. Oscillations of the profiles in the shock layer are dumped out when the equilibrium state $T_{xx} = T_{yy} = T_{zz}$ is established (at $z \approx -3.5$ in Fig. 1). As observed previously in dense gases and liquids [5,8,17], the longitudinal fluctuation $T_{zz}$ grows faster than the transverse ones. Notice that both $T_{xx}(z)$ and $T_{yy}(z)$ oscillate nearly in phase with the number density $\rho(z)$, stream velocity $u_z(z)$, potential energy $U(z)$, and internal energy $E(z)$ (excluding kinetic energy associated with the mass stream), but out of phase with $T_{zz}(z)$.

The pressure tensor is calculated by the Hardy's modification of microscopic formula of Irving and Kirkwood. The normal component $P_{zz}(z)$ of the pressure tensor and $2 \times$ shear-stress $2\tau = P_{zz} - \frac{1}{2}(P_{xx} + P_{yy})$ are also shown in Fig. 1. The first maximum of the shear stress is located at the center of initial shock ($z \approx 0$), whereas the second one corresponds to the first minimum in the pressure profiles. Thus the plastic flow under shock loading achieves its steady state through the shear relaxation process accompanied by oscillations. This contrasts

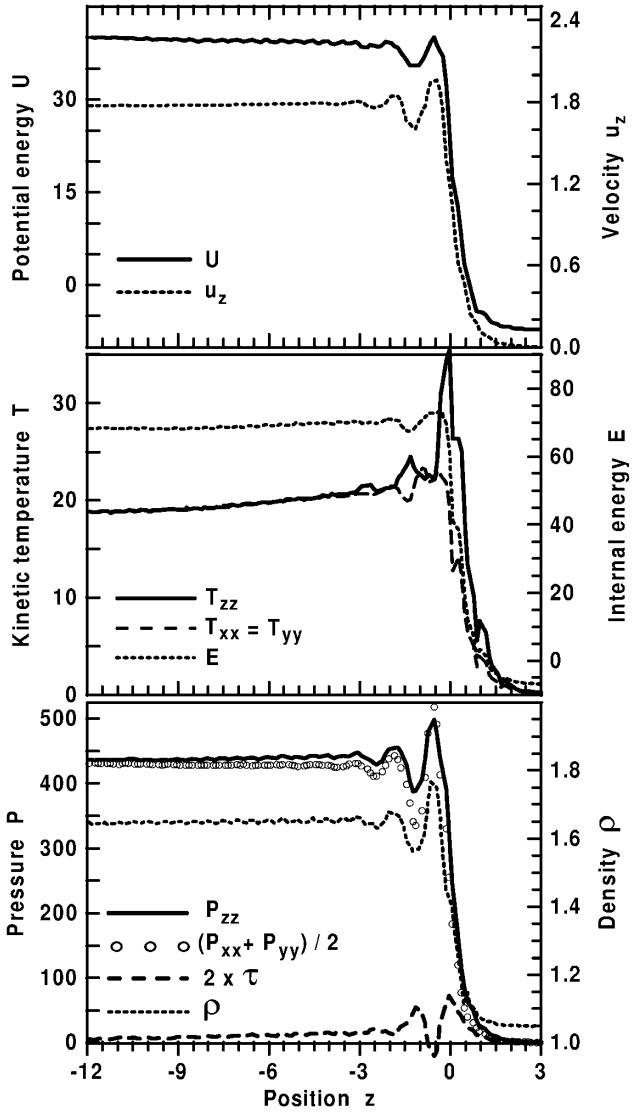


FIG. 1. Profiles $U(z)$, $u_z(z)$, $T_{zz}(z)$, $T_{xx}(z) = T_{yy}(z)$, $E(z)$, $P_{zz}(z)$, $[P_{xx}(z) + P_{yy}(z)]/2$, $P_{zz} - (P_{xx} + P_{yy})/2$, and $\rho(z)$ for a shock wave at Mach number $M = 4$ (averaged over 246 configurations from an ensemble). The bin width is $0.13\sigma$.

substantially with the viscous shear relaxation process in fluid shock waves. Hence, it follows that the strain rate has both elastic and plastic components even for strong shock waves ($u_p/c_0 \sim 1.5$) and that the oscillations within the shock front accompany the transition from elastic compression to plastic deformation. As shown in Table I, the ratio $\Delta P/\tau_{\max}$ estimated from our MD experiments is in reasonable agreement with the Holian conjecture in that it appears to be roughly 10 in 3D crystals [17,18]. Our previous simulation of fluid shock waves by the time-averaging technique exhibited ratios of 9.3 and 10.1 for Mach numbers $M = 3.25$ and 6.5, respectively [8].

To gain insight into kinetic features of the shock layer, we explored the evolution of velocity distribution functions across the shock front. Figure 2 gives the distribution of the longitudinal component $v_z$ for run $A$ in different bins of width $\sim 0.4\sigma$ normal to the $z$ axis. Initially, the high-energy thin tail is generated at the beginning of the shock front ($z > 0.6$). Then it grows in amplitude forming the downstream distribution due to the particle flux in velocity space. At maximum of the stream velocity ($z \approx -0.6$) it becomes nearly Maxwellian shifted somewhat into the region of greater $v_z$. On the other hand, it shifts into the region of smaller $v_z$ at the first minimum of $u_z(z)$ ($z \approx -1.2$). It is noteworthy that the distribution variance peaks at maximum of the $T_{zz}$ ($z \approx 0$) providing the physical interpretation for the "longitudinal temperature" maximum observed in previous works. We emphasize that the distribution functions of $v_z$ within the oscillation region behind the first peak in $u_z(z)$ are close to that of equilibrium distribution. In contrast, the distributions in bins located ahead of the first peak ($z > -0.6$) differ widely from the Maxwellian.

Figure 3 shows the evolution of the probability density for the potential energy across the shock layer. It is seen that the lattice rearrangement appears at the very beginning of the shock front ($z > 1.4$) forming a high-energy repulsive tail in the distribution. The corresponding change in the structure of the LJ crystal is demonstrated in Fig. 4, where the unsymmetrical pair distribution function $\rho^{[2]}(r; z)$, dependent on the distance $r$ in the $xy$ plane between two particles, is calculated in different bins normal to the $z$ axis (this function is given by $\rho^{[2]}(r; z) = \rho^{(2)}(r; z)/\rho^{(1)}(z) = \rho g(r)$ for a homogeneous system, where $g(r)$ is the radial distribution function). As can be seen from the figure, a new first neighbor peak at $r \approx 0.86$ begins to grow (along with broadening other peaks) before any significant disorder begins to emerge. Such a behavior is totally different from that observed in Ref. [8] for a shock wave in a liquid. It may be explained by elastical compression of the lattice

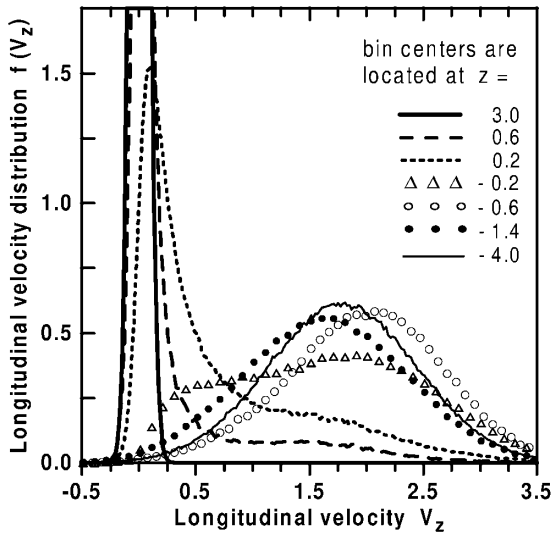


FIG. 2. Evolution of the longitudinal velocity distribution $f(v_z)$ across the shock layer, $M = 4$; the bin width is $0.4\sigma$.

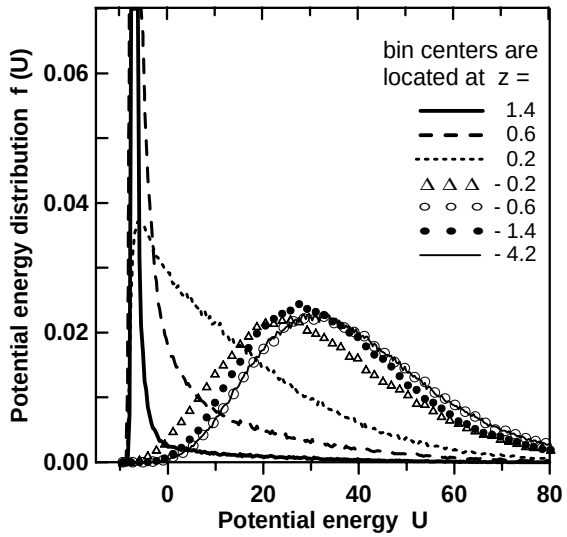


FIG. 3. Evolution of the potential energy distribution $f(U)$ across the shock layer, $M = 4$; the bin width is $0.4\sigma$.

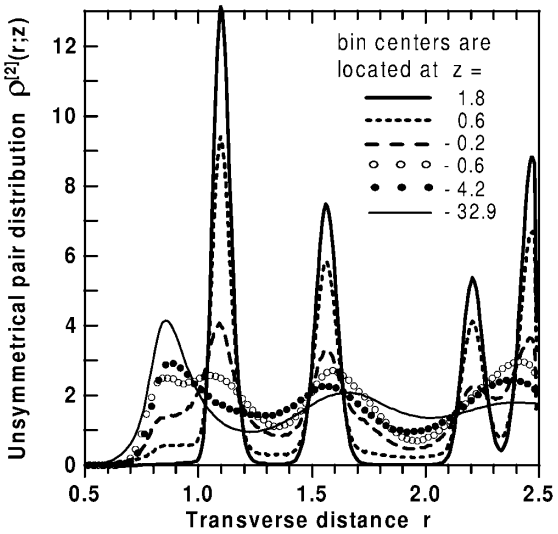


FIG. 4. Evolution of the unsymmetrical pair distribution $\rho^{[2]}(r; z)$ across the shock layer, $M = 4$; the bin width is $0.4\sigma$.

before relief of the shear stress coupled with creation of dislocations in the shock front region. One can also see that the location of this new first peak is almost not shifted when melting the LJ crystal, and that the shift of the first neighbor shell under strong shock compression exceeds those of other shells. The curve at $z = -32.9$ shows that an appreciable short-range order exists in the shock compressed fluid, as it was also observed in Ref. [8].

In summary, with these MD techniques developed for quantitative study of the shock wave structure, we have carried out the first systematic MD study of the oscillatory structure of shock waves in fcc LJ crystal and have captured the details of evolution of the velocity and potential energy distributions. We find that the longitudinal velocity distribution within the shock front is essentially different from the Maxwellian one. The simulations also reveal the details of crystal lattice transformation in the transition from elastic deformation to steady plastic flow under shock loading through the calculation of pair distribution functions.

The authors are grateful to B. L. Holian and P. S. Lomdahl for helpful discussions and to J. Belak for providing us with his report. The work was supported by Russian Foundation for Basic Research (Grant No. 98-02-16855) and Japan Society for Promotion of Science (ID No. P98042).

[1] L. D. Landau and E. M. Lifshitz, *Fluid Mechanics* (Pergamon Press, Oxford, 1959).
[2] H. W. Liepman, R. Narashima, and M. T. Chahine, Phys. Fluids **5**, 1313 (1962); C. Muckenfuss, *ibid.* **5**, 1325 (1962).
[3] H. M. Mott-Smith, Phys. Rev. **82**, 885 (1951); I. E. Tamm, Tr. Fiz. Inst. Akad. Nauk SSSR **29**, 317 (1965).
[4] S. Chapman and T. G. Cowling, *The Mathematical Theory of Non-Uniform Gases* (Cambridge University, Cambridge, England, 1960).
[5] V. Y. Klimenko and A. N. Dremin, in *Detonatsiya, Chernogolovka,* edited by O. N. Breusov *et al.* (Akademiya Nauk, Moscow, 1978), p. 79.
[6] B. L. Holian, W. G. Hoover, B. Moran, and G. K. Straub, Phys. Rev. A **22**, 2798 (1980); W. G. Hoover, Phys. Rev. Lett. **42**, 1531 (1979).
[7] M. Koshi, *et al.,* Kayaku Gakkaishi **55**, 229 (1994).
[8] S. I. Anisimov, V. V. Zhakhovskii, and V. E. Fortov, JETP Lett. **65**, 755 (1997); V. V. Zhakhovskii, K. Nishihara, and S. I. Anisimov, *ibid.* **66**, 99 (1997).
[9] E. Salomons and M. Mareschal, Phys. Rev. Lett. **69**, 269 (1992); B. L. Holian, C. W. Patterson, M. Mareschal, and E. Salomons, Phys. Rev. E **47**, R24 (1993).
[10] F. J. Uribe, R. M. Velasco, and L. S. García-Colín, Phys. Rev. E **58**, 3209 (1998); Phys. Rev. Lett. **81**, 2044 (1998).
[11] M. Al-Ghoul and B. C. Eu, Phys. Rev. E **56**, 2981 (1997).
[12] D. W. Brenner, D. H. Robertson, M. L. Elert, and C. T. White, Phys. Rev. Lett. **70**, 2174 (1993); *ibid.* **76**, 2202 (1996).
[13] B. L. Holian, Shock Waves **5**, 149 (1995).
[14] B. L. Holian and G. K. Straub, Phys. Rev. Lett. **43**, 1598 (1979); Phys. Rev. B **18**, 1593 (1978).
[15] V. Y. Klimenko and A. N. Dremin, Sov. Phys. Dokl. **25**, 288 (1980); Prog. Astronaut. Aeronaut. **75**, 253 (1981).
[16] J. Belak, LLNL Report No. UCRL-JC-109989, 1992.
[17] B. L. Holian, Phys. Rev. A **37**, 2562 (1988).
[18] B. L. Holian and P. S. Lomdahl, Science **280**, 2085 (1998).
[19] V. V. Zhakhovski, S. V. Zybin, K. Nishihara, and S. I. Anisimov, in *Proceedings of Symposium on Shock Waves* (Aoyama Gakuin University, Tokyo, 1999), pp. 241–244.
[20] Y. B. Zeldovich and Y. P. Raizer, *Physics of Shock Waves* (Academic, New York, 1966), Vols. I and II.